# Hydrogen permeability of diamondlike amorphous carbons

Motonori TamuraTai Kumagai

Citation: Journal of Vacuum Science & Technology A: Vacuum, Surfaces, and Films **35**, 04D101 (2017); doi: 10.1116/1.4977106

View online: http://dx.doi.org/10.1116/1.4977106

View Table of Contents: http://avs.scitation.org/toc/jva/35/4

Published by the American Vacuum Society

# Hydrogen permeability of diamondlike amorphous carbons

Motonori Tamura[a)]
*Center for Industrial and Governmental Relations, The University of Electro-Communications, 1-5-1 Chofugaoka, Chofu, Tokyo 182-8585, Japan*

Tai Kumagai
*TS Nanocoat Corporation 2-1-19 Surugadai, Kanda, Chiyoda-Ku, Tokyo 101-0062, Japan*

(Received 13 October 2016; accepted 7 February 2017; published 16 March 2017)

The hydrogen barrier properties of the coatings of nitride and diamondlike amorphous carbon (DLC) were evaluated. Using plasma chemical vapor deposition and sputtering, ZrN, TiAlN, AlCrN, CrN, and DLC coatings were deposited with a thickness of about 3 $\mu$m. It was confirmed that all coatings have an impact on decreasing the hydrogen permeation rate. Specifically, by coating stainless steel with a DLC coating, the hydrogen permeation rate was reduced to 1/1000 or lower compared to that without a coating. By providing a buffer layer of Cr-N, the hydrogen barrier function was improved. DLC coatings with high hydrogen content had an especially high hydrogen barrier function. For hydrogen diffusion in coatings, the movement of atoms through hydrogen trap sites is important. There are both $sp^3$ and $sp^2$ bonds in DLC coatings, and excess hydrogen can be found in the interstitial space and the above-mentioned hydrogen trap sites. It is suggested that the hydrogen trap sites in a DLC coating with high hydrogen content are likely already filled with hydrogen atoms, and the movement of new hydrogen atoms could be limited. 
[http://dx.doi.org/10.1116/1.4977106]

## I. INTRODUCTION

In many metallic materials such as carbon steel,[1–5] stainless steel,[6–9] and aluminum alloys,[10–12] hydrogen present in the material is well known to have a negative impact on the mechanical properties of the material. Among these materials, steel, which has an especially high mechanical strength, consisting of the ferrite and martensitic structure, has high hydrogen diffusivity, and it tends to show hydrogen embrittlement.[1–3] In recent years, there have been attempts to use hydrogen gas as an alternative to fossil fuels, and many hydrogen energy systems that use high-pressure hydrogen are being developed. The development of a technology for preventing degradation of materials by hydrogen is required. In particular, when steel is exposed to hydrogen gas, molecular hydrogen atomically dissociates on the surface of steel relatively easily, which attacks the material, causing hydrogen embrittlement.[4,5]

Studies on preventing hydrogen attack by barrier coatings have been conducted by researchers in various fields such as nuclear fusion reactors, fuel cells, $H_2S$-corrosion resistant parts, and vacuum equipment. Fine ceramic coatings such as $Al_2O_3$, TiC, TiN, and BN have been reported to be suitable as a hydrogen barrier. There are various methods of generating these coatings such as chemical vapor deposition (CVD), physical vapor deposition (PVD), and plasma-spray, and the deposition of ceramic coatings with a thickness of several micrometers can decrease hydrogen attack by several orders of magnitudes.[16–26]

Diamondlike carbon (DLC) coatings have superior properties such as high hardness, high resistance to abrasion, low friction, low aggressiveness against mating materials, seize resistance, high insulation, infrared transparency, high gas barrier properties, and biocompatibility.[27–34] Utilizing its low friction and low aggressiveness against mating materials, its application to sliding parts, such as in automobiles, is dominant.

DLC is an amorphous coating, which is a mixture of a diamond structure ($sp^3$ bond) and a graphite structure ($sp^2$ bond). The fraction of $sp^3$ bonds in DLC varies from 10% to 70%, and it also contains 0–60 at. % hydrogen; therefore, its density varies from 1.1 to 3.0 g/cm$^3$, leading to a variety of characteristics. If the amount of hydrogen is less than 25 at. %, the density, hardness, and abrasion resistance are high; therefore, these materials are used as cutting tools, molds, machinery parts, hard-disk heads, and magnetic tapes. DLC, with high hydrogen content, have a lower density and polymerlike characteristics.

The different compositional arrangements of DLC coatings are graphically represented in the form of a ternary phase diagram.[29–31]

The $sp^3$ bonding of DLC determines many beneficial properties of diamond, such as its mechanical hardness, chemical and electrochemical inertness, and wide band gap. Typical properties of the various forms of DLC are compared[30] to diamond and graphite. It is possible to produce DLCs by a wide range of vacuum deposition methods.[27–34] The $sp^3$ bonding of carbon in DLCs is a function of ion energy, and the highest $sp^3$ fractions are formed by $C^+$ ions with ion energy around 100 eV.[32]

There are generally two types of DLC coating methods: the PVD method in which films are formed from solid carbon through sputtering and cathodic arc discharge, and the CVD method that forms film by turning hydrocarbons such as $CH_4$ and $C_2H_2$ into plasma. Plasma used in the plasma CVD method can be generated through various types of discharges such as direct current, alternating current, radio

a)Electronic mail: mtamura@sangaku.uec.ac.jp

frequency, microwave, and electron cyclotron resonance. Diamond and graphite form under high temperature, but DLC is often formed at 300 °C or lower.

There are various types of DLC materials such as hydrogen-free DLC and metal-doped DLC (that is doped with metallic elements). Because of its low friction and low aggressiveness of DLC materials against mating materials, its application to sliding parts, such as in automobile parts, is widespread. For protecting the global environment and for realizing $CO_2$ reduction, improvement in fuel efficiency, prevention of abnormal noises, oil reduction, and improvement in durability are being attempted.[27]

There is an example of DLC coating the insides of a polyethylene terephthalate (PET) bottle, acting as a gas barrier, through which permeation of oxygen and moisture is suppressed.[33] This helps long-term maintenance of the quality of the products in the bottle.[34] The inside of PET bottles is coated with a plasma process that uses hydrocarbon gas as the source material. The coating thickness is 10–40 nm and has a slight yellow tint. The composition of the coating is 50%–60% carbon atoms and 40%–50% hydrogen atoms, and its density is 1.2–1.6 g/cm$^3$. DLC bottles show a 12–20 times improvement in the oxygen barrier property compared to that of untreated bottles. In addition, carbon dioxide gas barrier properties can be improved ten times or more in coated 500 ml DLC bottles. Furthermore, if we evaluate the sorption of flavor based on the difference in the carbon number, the flavor barrier improved three to six times for esters and aldehydes (C6, C8, and C10), and 20 times or more for alcohols.[34]

As such, a DLC coating has a wide range of applications, but tests on hydrogen barrier functions are quite limited.[35–37] It has been reported that when a test method for hydrogen permeation was established and applied to one type of prepared DLC coating, it showed hydrogen barrier characteristics.[35,38] However, the relationship among each structure of a DLC coating, the hydrogen content, and the hydrogen gas barrier function have still not been understood.

In this study, the relationship between various characteristics of a DLC coating and the hydrogen barrier function was focused, especially the hydrogen content in the coating, in order to examine their interrelation.

## II. EXPERIMENT

### A. Deposition process

Coatings were prepared using plasma CVD and a sputtering method (Fig. 1). DLC coatings, and ZrN, TiAlN, CrN, and AlCrN coatings with a thickness of about 3 $\mu$m were deposited on Type 316L stainless steel. About 0.6 $\mu$m thick Cr-N coating (Cr+CrN) was used as a buffer layer under DLC coatings. This buffer layer is necessary to increase the adhesiveness of the DLC coating to the stainless steel substrate. A Cr layer (0.1 $\mu$m) was deposited immediately above the stainless steel, and a CrN (0.5 $\mu$m) coating was deposited on top of this Cr layer. Three DLC coatings were prepared with different hydrogen content (20%, 10%, and 8%) on the same buffer layer. DLC coatings with hydrogen content of

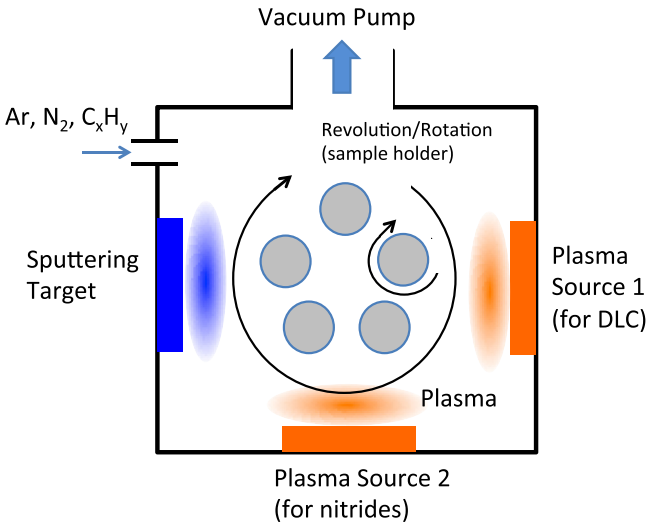


FIG. 1. (Color online) Schematic illustration of hybrid coating system of sputtering and CVD.

20% and 10% were prepared using plasma CVD, and the coating with hydrogen content of 8% was prepared using sputtering. The composition of TiAlN (atomic molar ratio) was Ti:Al = 1:1. The AlCrN composition was Al:Cr = 7:3.

### B. Characterization of coatings

Measurement of coating thickness and the microstructure of the surface of the coating and its cross section were observed using scanning electron microscopy, and transmission electron microscopy (TEM). Hydrogen content in the DLC coating before and after the hydrogen permeation test was measured using elastic recoil detection analysis. Structural analysis of the DLC coating before and after the hydrogen permeation test was performed and compared by Laser Raman Spectroscopy.

### C. Hydrogen-permeation tests

Hydrogen-permeation tests were performed on the coated Type 316L stainless steel samples. These tests were based on the differential-pressure methods described in ISO15105-1:2007, the international standard for determination of gas-transmission rates. This part of the standard specifies two methods for determining the gas-transmission rate of a single-layered plastic film or sheet and multilayered structures under a differential pressure. One method uses a pressure sensor, the other a gas chromatograph, to measure the amount of gas permeating through a test specimen. In this study, a gas chromatograph was used.

Figure 2 shows a schematic illustration of the apparatus. The coated samples (diameter: 35 mm; thickness: 0.1 mm) were set on a silicon fiberglass susceptor, which was porous and could be held in place without bending at temperatures up to 773 K. The apparatus was evacuated to $10^{-6}$ Pa. After the test temperature stabilized, hydrogen (purity of 99.995%) was introduced into the susceptor side of the chamber at a filling pressure of 400 k Pa. The stainless-steel-sample side of the apparatus was continuously evacuated. The samples were

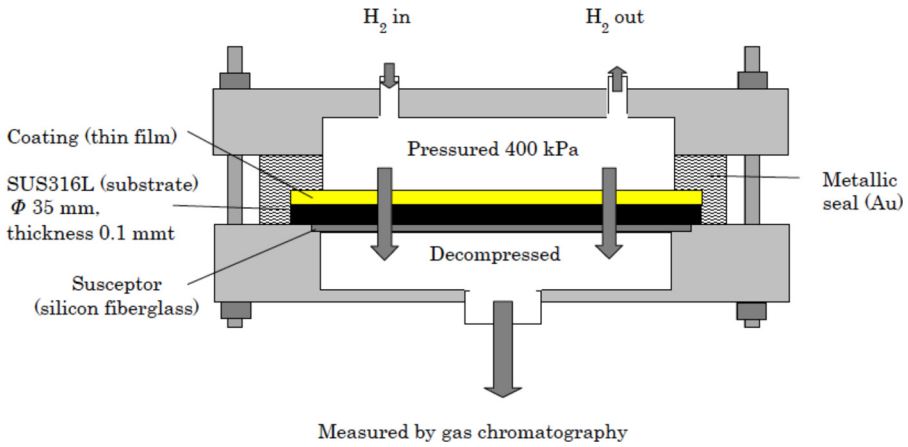


FIG. 2. (Color online) Schematic illustration of the experimental apparatus for hydrogen-permeation measurements.

affixed with a metallic seal made of gold and could be heated by an electric furnace to 773 K without oxidation. The permeation area was 6.6 $cm^2$.

A thermal-conductivity detector (TCD) and a flame-ionization detector were used with the gas chromatograph. The TCD consisted of four tungsten filaments in a temperature-controlled cell; this type of detector senses changes in the thermal conductivity of the column effluent and compares them to the flow of the carrier gas.

The permeability, $\Phi$, is generally defined by the expression[25,35–38]

$$\Phi = J \cdot d/A \cdot \Delta p^n, \quad (1)$$

where $J$ is the permeation flux of hydrogen through a sample of area $A$ and thickness $d$, under a partial pressure gradient $\Delta p$ across the sample called the driving pressure. The exponent $n$ represents different permeation regimes: diffusion-limited and surface-limited when $n = 0.5$ and 1, respectively. Hydrogen permeation through a thin-film-coated steel sample is known to be diffusion-limited when the driving pressure is between $10^4$ and $10^5$.[17,25] According to our previous experiments, the hydrogen permeation through DLC coatings was diffusion-limited ($n = 0.5$).

The permeation flux was continuously measured at a test temperature and under a test hydrogen pressure. Under a hydrogen pressure of 400 k Pa, for example, the standard deviation decreased below 10% among the data for permeation flux, through the noncoated stainless steel substrate after 30 min at 773 K, or through DLC coated stainless steels after 60 min at 573 K. In this study, hydrogen permeation data after 90 min when the samples reached to a test temperature were plotted on figures.

## III. RESULTS AND DISCUSSION

### A. Hydrogen-permeation mode

The permeation of hydrogen through solid materials proceeds via adsorption, dissociation, diffusion, and recombination coupled with desorption.[39–47] Figure 3 shows a schematic illustration of hydrogen permeation in coated samples. A hydrogen molecule ($H_{2,ad}$) is adsorbed on the surface of the film and decomposes to hydrogen atoms ($H_{ad}$). Such adsorbed hydrogen atoms diffuse into the film from the film surface ($H_{film,in}$) and move toward the interface with the substrate ($H_{film,out}$). Hydrogen atoms diffuse into the substrate from the interface of the film ($H_{sub,in}$) to the noncoated side of the substrate ($H_{sub,out}$). At the noncoated side of the substrate, the hydrogen atoms ($H_{des}$) form hydrogen molecules and desorption occurs. In this study, a driving force of hydrogen permeation was the pressure difference between the high- and low-pressure sides. Hydrogen permeation occurred in the film and the substrate because of decompression in the gas phase at the noncoated side of the substrate.

Our previous study has demonstrated the dependence of permeation flux $J$ on the driving pressure$\Delta p$ in BN- and TiN-coated samples[17] and DLC coatings. The exponent $n$ had a value of 0.48–0.55 at 573–773 K, which indicated that hydrogen passed through the samples in the diffusion-limited permeation mode. When $n = 0.5$ (diffusion-limited regime) in Eq. (1), the overall permeation flux of hydrogen through the sample can be given by Fick's law. In a steady state, the overall permeation flux $J$ (measured in mol $s^{-1}$) through a sample of thickness $d_{film} + d_{sub}$ ($d_{film}$, thickness of film: $1.5 \times 10^{-6}$ m; $d_{sub}$, thickness of substrate: $1.0 \times 10^{-4}$ m) and area $A$ ($6.6 \times 10^{-4}$ $m^2$) is expressed as

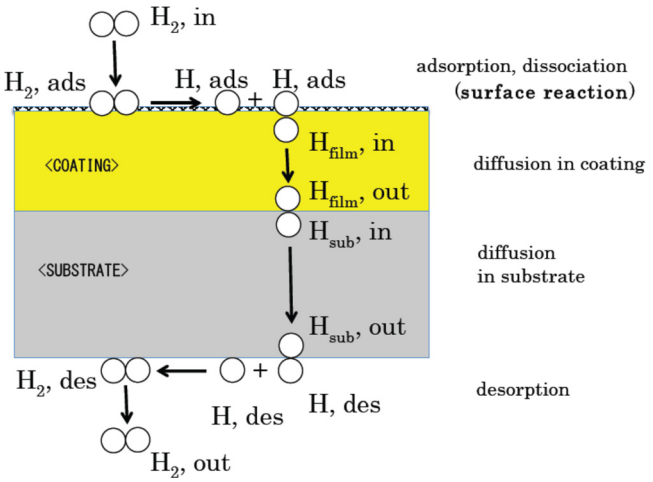


FIG. 3. (Color online) Schematic illustration of the permeation mechanism.

$$J = \Phi \cdot A\left((P_{\mathrm{H2,in}})^{0.5} - (P_{\mathrm{H2,out}})^{0.5}\right)/(d_{\mathrm{film}} + d_{\mathrm{sub}}), \qquad (2)$$

where $\phi$ is the permeability of the sample as shown before, and $P_{\mathrm{H2,in}}$ ($4.0 \times 10^5$ Pa) and $P_{\mathrm{H2,out}}$ ($1.0 \times 10^{-6}$ Pa) are the hydrogen pressures at the feed side and at the vacuum-pumping side, respectively.

### B. Hydrogen permeation characteristics of each type of coating

Hydrogen permeation test results for each type of coating are shown in Fig. 4. ZrN, TiAlN, AlCrN, CrN, and DLC coatings that contains 20% hydrogen [DLC (20%$H_2$) in Fig. 4] lower the hydrogen permeation rate by 2 orders of magnitude (1/100 or lower) compared to the base material (SUS316L in the figure). Specifically, DLC (20%$H_2$) lowered the hydrogen permeation rate by three orders of magnitudes (1/1000 or lower) at measurement temperatures of 573, 673, and 773 K. The temperature dependence of hydrogen permeation rate was different in each nitride coating. It is suggested that temperature dependence of activation energy of hydrogen diffusion in CrN was low.

The relationship between the characteristics and the hydrogen permeation rate of DLC coating will be discussed in detail in the next section.

### C. Characteristics and hydrogen barrier function of DLC coating

Hydrogen permeation test results for the DLC coating are shown in Fig. 5. DLC coatings with varying hydrogen content (20, 10, and 8 at. %) were compared.

Compared to the base material, all coatings reduced the hydrogen permeation rate by two or more orders of magnitude, showing a superior hydrogen barrier function. The DLC coating with higher hydrogen content has a lower hydrogen permeation rate.

The buffer layer (0.1 $\mu$m thick Cr and 0.5 $\mu$m thick CrN) also shows a hydrogen barrier function. When there is no buffer layer [DLC (20%$H_2$) without buffer layer in Fig. 5],

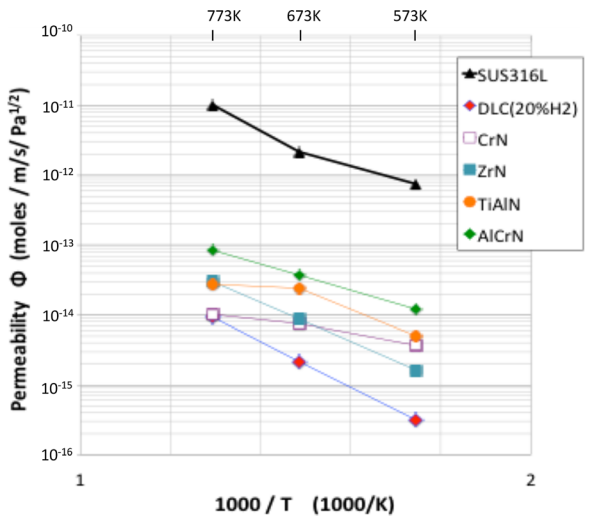


FIG. 4. (Color online) Arrhenius plot of hydrogen permeability of SUS316L and coated SUS316L by nitrides and DLC as a function of temperature.

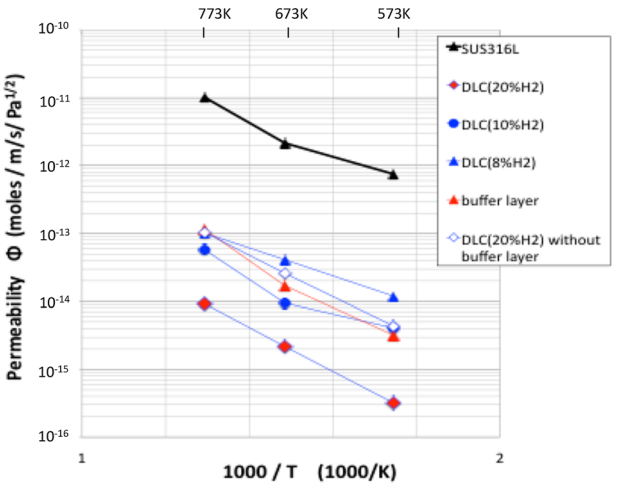


FIG. 5. (Color online) Arrhenius plot of hydrogen permeability of DLC coatings.

the hydrogen permeation rate becomes high by an order of magnitude. The combination of the buffer layer and the DLC coating [DLC (20%$H_2$)] had the lowest hydrogen permeation rate.

The TEM cross-sectional observation results of the DLC coating with a hydrogen content of 20% [DLC (20%$H_2$)] are shown in Fig. 6. The observed thickness of the DLC coating was 2.5 $\mu$m, and there was no diffraction pattern that indicates crystallinity; thus, the coating was confirmed to be amorphous. The buffer layer consists of two layers, and there is a 0.1 $\mu$m thick metallic Cr coating immediately above the substrate, and above this coating, there is a 0.5-$\mu$m thick CrN coating.

Hydrogen contents before and after the hydrogen permeation test for the three DLC coatings with varying hydrogen content are shown in Fig. 7. The hydrogen content of the DLC coating generated with the plasma CVD did not change notably after the hydrogen permeation test compared to the value before the test (Fig. 7). In the hydrogen permeation test, as discussed earlier, the DLC coating side is exposed to a 400 k Pa hydrogen gas atmosphere, while the backside of the stainless steel plate, the base material, is ventilated to vacuum. This difference in the hydrogen pressure becomes the driving force for hydrogen diffusion in the coatings. Test temperatures were 773, 673, and 573 K, each maintained for 2 h. It is equivalent to a test sample being annealed at this temperature in a hydrogen atmosphere. In particular, in the hydrogen permeation test, the sample is heated at 773 K, and the structural change in the DLC coating described next will occur. Figure 7 indicates that no large change in the hydrogen content occurs in all the DLC coatings even when their structures change.

When considering the hydrogen diffusion in DLC coatings, the structure of the DLC coating, the conditions of the hydrogen atoms, and the mechanism of hydrogen diffusion need to be considered. Based on the existing data, the hydrogen content before and after the hydrogen permeation test in this study and measurements of the structural changes using laser Raman spectroscopy, we discuss the factors for

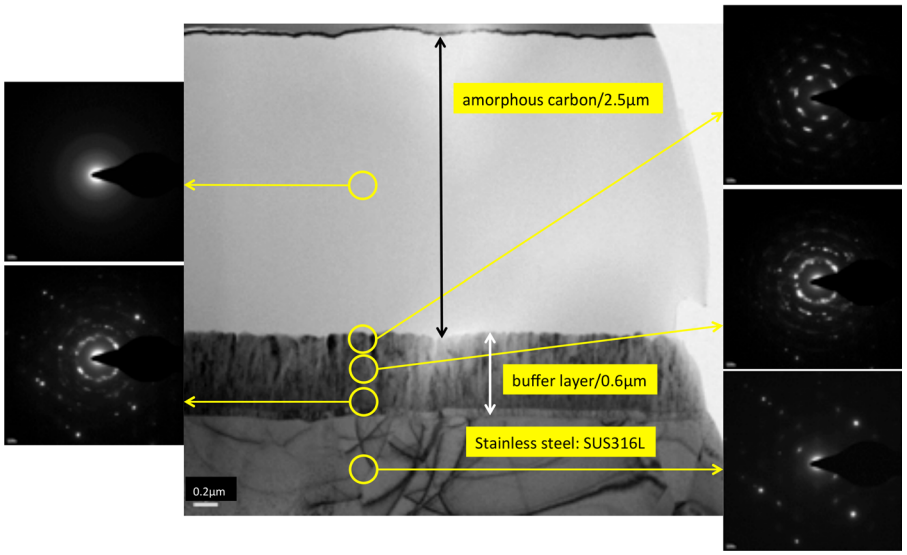


FIG. 6. (Color online) TEM image of cross section of DLC coated stainless steel.

achieving high hydrogen barrier ability of the DLC film with high hydrogen content.

When considering the structure of a DLC coating based on the local structure at the atomic level of the coating, it was determined that carbon atoms with a $sp^3$ hybrid orbital corresponding to the diamond structure, and carbon atoms with a $sp^2$ hybrid orbital corresponding to the graphite structure are mixed together.

It is known that the ratio of these $sp^2$ and $sp^3$ hybrid atoms strongly affects the various properties of the DLC coatings. The bond ratio of $sp^2$ and $sp^3$ atoms in DLC coatings is a strong indicator of the structure of DLC coatings. Various methods have been used to determine the bond ratio of $sp^2$ and $sp^3$ atoms in DLC coatings, such as laser Raman spectroscopy, photoelectron spectroscopy, electron energy loss spectroscopy, and x-ray absorption fine structure. In this study, we used laser Raman spectroscopy because of its ease in sampling data and usefulness of the obtained structural information.

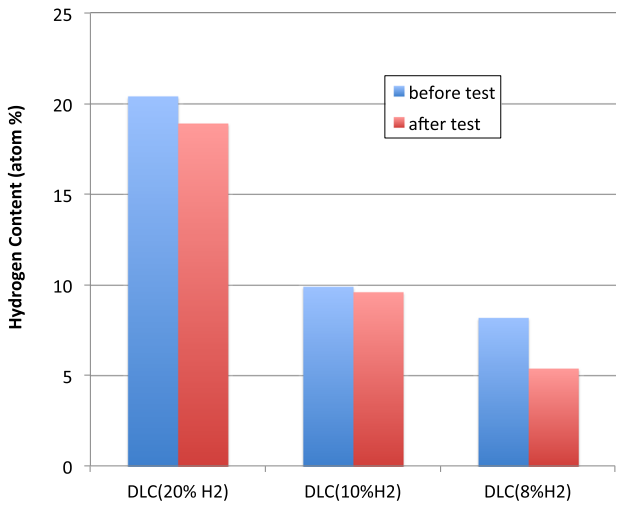


FIG. 7. (Color online) Hydrogen contents of DLC coatings before/after the hydrogen permeation tests at 773 K.

Raman spectral waveforms before and after the hydrogen permeation test, and Raman spectral waveform separation peak intensity comparison are shown in Figs. 8 and 9. Because of the heating up to 773 K in the hydrogen permeation test, the graphite structure increased in all the films. The obtained Raman spectral waveforms are separated into the G-band peak near 1350 $cm^{-1}$, derived from the graphite structure and a D-band peak near 1550 $cm^{-1}$, derived from disordered graphite, and the I(G)/I(D) intensity ratio was compared (Fig. 9). Visible light Raman spectroscopy has low sensitivity to the $sp^3$ bond, and can be considered as an evaluation of the $sp^2$ bond. However, in a sample after the hydrogen permeation rate test, with heating up to 773 K, the G-band peak increased notably, and fraction of graphite structure increased. Even when the hydrogen content is different, by heating to 773 K, it stabilizes into similar structures [i.e., the same I(G)/I(D) ratio].

As shown above, when the DLC coating is heated at 773 K, the fraction of graphite structure increases. This is consistent with existing reports.[53,54] However, as shown in Fig. 7, even when the structure changes, the hydrogen content does not change significantly. As hydrogen is assumed to be widely distributed in hydrogen trap sites such as interstitial spaces, pores, and dislocations in addition to bonding with carbon in the DLC coatings, even if part of the carbon structure changes, it likely does not have a strong impact on the overall hydrogen content.

One model can be proposed next to understand above data concerning structure and hydrogen content in DLC coatings.

Next, we discuss the state of hydrogen and the mechanism of hydrogen diffusion. Many studies on hydrogen diffusion in materials are on the behavior of hydrogen in a metal, and studies on hydrogen traps could be used as a reference.

Generally, similar to elemental diffusion in metals,[1–15,48–52] the rate of hydrogen diffusion in coatings is limited by the movement of atoms through hydrogen trap sites such as crystal defects (atomic pores or voids, dislocations, and crystal grain boundaries).

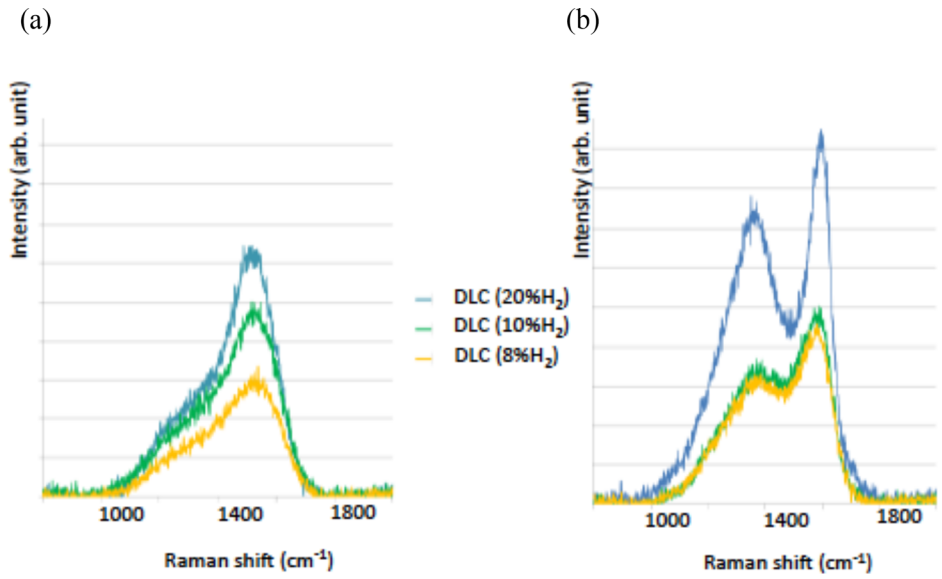


FIG. 8. (Color online) Raman shift of DLC coated samples (a) before the hydrogen permeation tests and (b) after the hydrogen permeation tests at 773 K.

Studies on hydrogen diffusion in the material, associated with the state of hydrogen in iron steel and hydrogen embrittlement mechanism are common, and there have been active studies since 1970s. The solid solubility and limit of the amount of hydrogen in a crystal lattice are obtained from the amount of hydrogen in a pure iron sample in equilibrium with a high-purity hydrogen gas environment.[1–4] Solid solubility is the ratio of hydrogen atoms to the number of normal lattice points, but hydrogen concentration is known to be proportional to the square root of hydrogen gas pressure. Hydrogen solid solubility in iron steel is dependent on the purity of the sample or the surface condition.[1–5]

The pathway for elemental diffusion in materials may include surface diffusion, lattice diffusion, grain boundary diffusion, and dislocation diffusion. Surface diffusion and grain boundary diffusion often have higher diffusion coefficients than lattice diffusion and dislocation diffusion. Studies on the state of hydrogen in metallic materials and the diffusion mechanism indicate that hydrogen diffusion progresses through hydrogen trap sites in materials.[1–15,48–52] Surface diffusion and grain boundary diffusion often have higher diffusion coefficients than lattice diffusion and dislocation diffusion. Lattice defects (atomic pores or voids, dislocations, and crystal grain boundaries), impurity atoms, precipitates, and interfaces with inclusions are proposed as hydrogen trap sites. These trap sites are schematically shown in Fig. 10. Activation energy of reversible hydrogen traps at grain boundaries, dislocations, and microvoids in iron or steels is reported to be lower than irreversible hydrogen traps around carbides or sulfides such as TiC and MnS,[40] as shown in Table I. Reversible hydrogen traps such as grain boundaries or ferrite interface can be effective function of hydrogen diffusion.

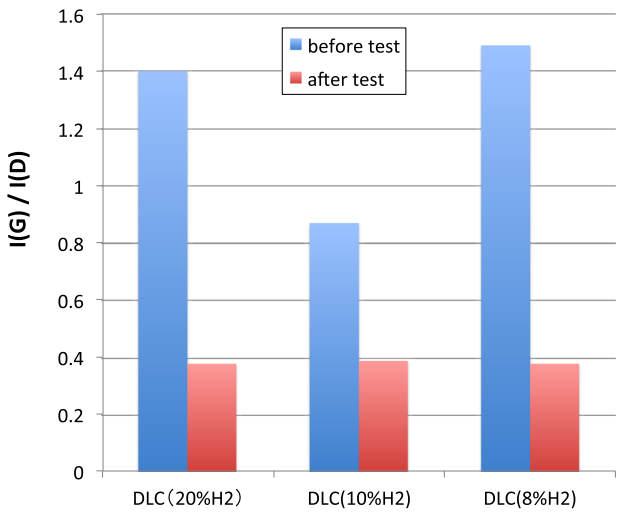


FIG. 9. (Color online) Raman intensity ratio of DLC coatings. I(G) corresponds to intensity of G-band peak near 1350 $cm^{-1}$, derived from the graphite structure and I(D) corresponds to a D-band peak near 1550 $cm^{-1}$, derived from disordered graphite.

Based on the bond energy between these trap sites and hydrogen, the state of hydrogen can be analyzed using thermal desorption spectroscopy.[52] Schematics of the potential energy for hydrogen in metallic materials are shown in Fig. 11. In trap sites, the potential energy is low and it becomes

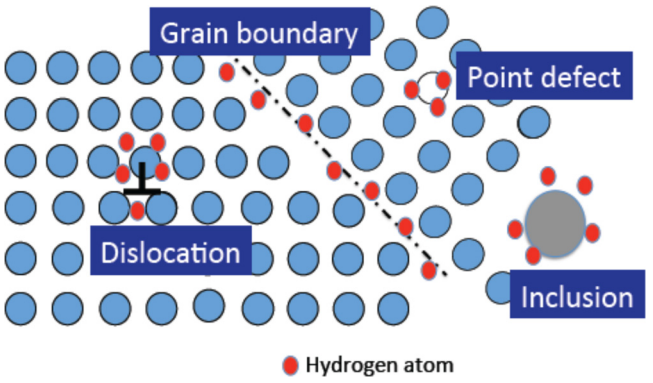


FIG. 10. (Color online) Hydrogen trap sites in metals.

TABLE I. Activation energy of hydrogen traps in iron and steels.

| Type of trap | Peak temperature (K) | Activation energy (kJ/mol) | Heating rate (K/min) | Material |
|---|---|---|---|---|
| Reversible hydrogen traps | | | | |
| Grain boundaries | 385.15 | 17.2 | 3 | Pure iron |
| Dislocations | 488.15 | 28.8 | 3 | Pure iron |
| Microvoids | 578.15 | 35.2 | 3 | Pure iron |
| Retained austenite | ~493.15 | — | 2.6 | High carbon steel |
| TiC (semicoherent) | ~503.15 | — | 1.7 | Low carbon steel |
| Ferrite/$Fe_3C$ interface | ~393.15 | 18.4 | 2.6 | Medium carbon steel |
| Irreversible hydrogen traps | | | | |
| TiC (incoherent) | ~983.15 | 86.9 | 3 | Medium carbon steel |
| MnS | ~768.15 | 72.3 | 3 | Low alloy steel |
| $Fe_3C$ (incoherent) | — | 84 | 4 | Medium carbon steel |
| Retained austenite | ~873.15 | 55 | 4 | Dual phase steel |

more stable. When the bond energy of the trapped hydrogen because of factors that lead to diffusion with a large concentration gradient is exceeded, movement of atoms progresses again; or in case of hydrogen environment embrittlement, it acts to extend cracks, leading to breakage. If there are more trap sites compared to the number of diffused atoms, the movement of atoms through the hydrogen trap site controls the rate of diffusion.

In ionic and shared bonds such as ceramic coatings, hydrogen diffusion in iron steel is several orders of magnitudes lower,[18,19,26] and it contains more lattice defects and impurity atoms than metallic materials. Hydrogen trap sites may function in ceramic coatings as well.

A DLC film is an amorphous material with mixed $sp^3$ and $sp^2$ bonds, but there also are pores and dislocations in graphite structure domain ($sp^2$) or diamond structure domain ($sp^3$), which can be considered as a type of crystal defect.[27,29,30,34] In a DLC film with high hydrogen content, hydrogen atoms have likely already filled these crystal defects, and the movement of new hydrogen atoms through the hydrogen trap sites in the coating was limited.

Figure 12 shows a schematic of the DLC coating structure prepared in this study, which has relatively high hydrogen content (10–30 at. % is assumed). There are mixed $sp^3$ and $sp^2$ bonds, and a localized compressional structure may also exist. The compressional structure of DLC coatings with high hydrogen content has been reported using TEM observations.[55] In addition, the structure calculated by computational science indicates the potential for a stable existence of excess hydrogen in areas that are structurally sparse.[56,57] Hydrogen may bond with carbon, exist in interstitial space, or be trapped in crystal defects such as atomic pores. When heated to 773 K, the bonding state between carbon-carbon and carbon-hydrogen partially changes to a graphite structure, but it does not significantly change the state of hydrogen in the crystal defects such as interstitial spaces and atomic pores. As for the diffusion coefficient in each mechanism in metallic materials, the diffusion rate because of crystal defects such as atomic pores and dislocations is an order of magnitude lower than that of interstitial spaces, and it often controls the rate of the diffusion process.[58] Mechanism of hydrogen movement can be different between metallic crystalline materials and amorphous materials. Studies focused on crystal defects or hydrogen traps will be important for hydrogen diffusion in DLC coatings in the future.

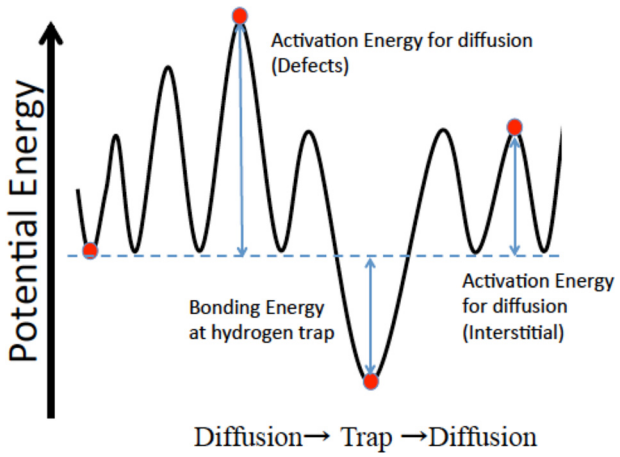


FIG. 11. (Color online) Schematic diagram of potential energy of hydrogen atoms in metals.

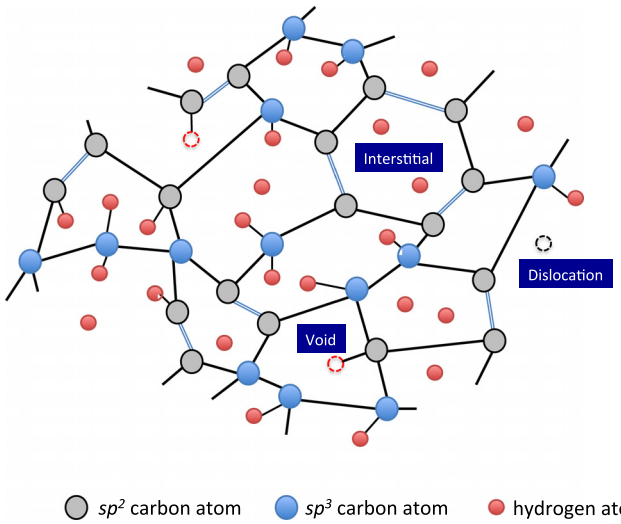


FIG. 12. (Color online) Schematic illustration of atomic structure of DLC rich in hydrogen.

In DLC coatings with high hydrogen content, hydrogen trap sites are likely filled with hydrogen already, and the movement (diffusion) of new hydrogen atoms through trap sites could be limited in the coating.

## IV. SUMMARY AND FUTURE DIRECTIONS

The hydrogen barrier properties of Type 316L stainless steels coated with nitride coatings and DLC coatings were evaluated.

Using plasma CVD and sputtering, ZrN, TiAlN, AlCrN, CrN, and DLC coatings were prepared with a thickness of about 3 $\mu$m. The results showed that all coatings lowered the hydrogen permeation rate significantly. By applying a buffer layer of Cr-N to DLC coatings, the hydrogen barrier properties were improved. A DLC coating with high hydrogen content was shown to have especially high hydrogen barrier properties. It is suggested that hydrogen trap sites are likely filled with hydrogen already in DLC coatings with high hydrogen content, and the movement (diffusion) of new hydrogen atoms through trap sites could be limited in the coating. Further study is necessary to understand completely the relation between hydrogen permeation behavior and structure in the DLC coatings.

Hydrogen in the DLC coating has an impact on the bonding state of carbon, and as a result, it changes its density and hardness. When the hydrogen content is low, the density and hardness increases. Since its resistance to abrasion is also high, it is widely used in cutting tools, molds, machinery parts, hard-disk heads, magnetic tapes, etc. The industrial application of DLC coatings with high hydrogen content was previously limited, but new applications as a coating with hydrogen barrier properties is expected to be developed in the future.


[1]A. R. Troiano, Trans. Am. Soc. Met. **52**, 54 (1960).
[2]C. D. Beachem, Metall. Trans. **3**, 441 (1972).
[3]J. P. Hirth, Metall. Trans. A **11**, 861 (1980).
[4]M. Nagumo, M. Nakamura, and K. Takai, Metall. Trans. A **32**, 339 (2001).
[5]K. Takai, Y. Homma, K. Izutsu, and M. Nagumo, J. Jpn. Inst. Met. **60**, 1155 (1996).
[6]M. B. Whiteman and A. R. Troiano, Corrosion **21**, 53 (1965).
[7]C. L. Briant, Metall. Trans. A **10**, 181 (1979).
[8]S. Fukuyama, K. Yokogawa, K. Kubo, and M. Araki, Trans. Jpn. Int. Met. **26**, 325 (1985).
[9]G. Han, J. He, S. Fukuyama, and K. Yokogawa, Acta Mater. **46**, 4559 (1998).
[10]S. Osaki, D. Itoh, and M. Nakai, J. Jpn. Inst. Light Met. **51**, 222(2001).
[11]M. Ando, M. Senoo, and M. Kanno, J. Jpn. Inst. Light Met. **57**, 19 (2007).
[12]G. A. Youg, Jr. and J. R. Scully, Metall. Mater. Trans. A **33**, 101 (2002).
[13]C. San Marchi, B. P. Somerday, and S. L. Robinson, Int. J. Hydrogen Energy **32**, 100 (2007).
[14]S. K. Lee, H. S. Kim, and S. J. Noh, J. Korean Phys. Soc. **5**, 3019 (2011).
[15]K. Horikawa, H. Okada, H. Kobayashi, and W. Urushihara, J. Jpn. Inst. Met. **74**, 199 (2010).
[16]M. Tamura and K. Shibata, J. Jpn. Inst. Met. **69**, 1039 (2005).
[17]M. Tamura, M. Noma, and M. Yamashita, Surf. Coat. Technol. **260**, 148 (2014).
[18]J. Yamabe, S. Matsuoka, and Y. Murakami, Int. J. Hydrogen Energy **38**, 10141 (2013).
[19]R. Checchetto, M. Bonelli, L. M. Gratton, A. Miotello, A. Sabbioni, L. Guzman, Y. Horino, and G. Benamati, Surf. Coat. Technol. **83**, 40 (1996).
[20]S. Sarkar, S. Datta, S. Das, and D. Basu, Surf. Coat. Technol. **204**, 391 (2009).
[21]C. Shan, A. Wu, Y. Li, Z. Zhao, Q. Chen, Q. Huang, and S. Shi, J. Nucl. Mater. **191–194**, 221 (1992).
[22]R. G. Song, Surf. Coat. Technol. **168**, 191 (2003).
[23]G. Zhang, S. Dou, Y. Lu, Y. Shi, X. Lai, and X. Wang, Int. J. Hydrogen Energy **39**, 610 (2014).
[24]N. Lee, S. Lee, K. Kim, W. Kim, H. Ju, D. M. Kim, and T. Hong, Int. J. Hydrogen Energy **38**, 7654 (2013).
[25]T. Chikada, A. Suzuki, Z. Yao, D. Levchuk, H. Mainer, T. Terai, and T. Muroga, Fusion Eng. Des. **84**, 590 (2009).
[26]G. W. Hollenberg, E. P. Simonen, G. Kalinin, and A. Terlain, Fusion Eng. Des. **28**, 190 (1995).
[27]N. Terayama, J. Plasma Fusion Res. **87**, 548 (2011).
[28]A. Zeng, V. F. Neto, J. J. Gracia, and Q. H. Fan, Diamond Relat. Mater. **43**, 12 (2014).
[29]W. Jacob and W. Moller, Appl. Phys. Lett. **63**, 1771 (1993).
[30]J. Robertson, Mater. Sci. Eng. **R37**, 129 (2002).
[31]J. Robertson, Prog. Solid State Chem. **21**, 199 (1991).
[32]M. Weiler, S. Sattel, K. Jung, H. Ehrhardt, V. S. Veerasamy, and J. Robertson, Appl. Phys. Lett. **64**, 2797 (1994).
[33]N. Boutroy *et al.*, Diamond Relat. Mater. **15**, 921 (2006).
[34]T. Kage, J. Vac. Soc. Jpn. **58**, 330 (2015).
[35]A. Hatta, S. Kaneko, and M. K. Hassan, Plasma Process. Polym. **4**, S241 (2007).
[36]A. Hatta and H. Matsuhisa, New Diamond Front. Carbon Technol. **14**, 351 (2004).
[37]J. M. Lackner, W. Waldhauser, and M. Kahn, Acta Phys. Pol. A **4**, 1236 (2015).
[38]E. Serra and A. Perujo, J. Nucl. Mater. **258**, 1028 (1998).
[39]A. Diaz, J. M. Alegre, and I. I. Cuesta, Procedia Eng. **160**, 223 (2016).
[40]B. A. Szost, R. H. Vegter, and P. E. J. Rivera-Diaz-del-Castillo, Metall. Mater. Trans. A **44**, 4542 (2013).
[41]R. Hurlbert and J. O. Konecny, J. Chem. Eng. Phys. **34**, 655 (1961).
[42]A. Caravella, F. Scura, G. Barbieri, and E. Drioli, Chem. Eng. Sci. **63**, 2149 (2008).
[43]S. T. Oyama, M. Yamada, T. Sugawara, A. Takagaki, and R. Kikuchi, J. Jpn. Pet. Inst. **54**, 298 (2011).
[44]P. L. Andrew and A. A. Haasz, J. Appl. Phys. **72**, 2749 (1992).
[45]A. Pisarev, V. Shestakov, R. Hayakawa, Y. Hatano, and K. Watanabe, J. Nucl. Mater. **320**, 214 (2003).
[46]P. J. MacGuiness, M. Ceekada, V. Nemanic, B. Zajec, and A. Recnik, Surf. Coat. Technol. **205**, 2709 (2011).
[47]S. K. Lee, H. S. Kim, and S. J. Noh, J. Korean Phys. Soc. **59**, 3019 (2011).
[48]C. V. Di Leo and L. Anand, Int. J. Plasticity **43**, 42 (2013).
[49]R. Koyama and G. Itoh, Trans. Nonferrous Met. Soc. China **24**, 2102 (2014).
[50]A. Oudriss, J. Creus, J. Bouhattate, E. Conforto, C. Berziou, C. Savall, and X. Feaugas, Acta Mater. **60**, 6814 (2012).
[51]N. Yazdipour, D. Dunne, and E. Perelome, Mater. Sci. Forum **706–709**, 1568 (2012).
[52]K. Takagi, Sanyo Tech. Rep. **22**, 14 (2015).
[53]A. Shimizu and M. Kawaguchi, Bull. TIRI **9**, 68 (2014).
[54]P. Yang, S. C. H. Kwok, R. K. Y. Fu, Y. X. Leng, J. Wang, N. Huang, Y. Leng, and P. K. Chu, Surf. Coat. Technol. **177–178**, 747 (2004).
[55]K. Sasagawa, Koperunikusu **10**, 3 (2001).
[56]A. Erdemir and O. Wryilmaz, Friction **2**, 140 (2014).
[57]F. Rose *et al.*, J. Appl. Phys. **116**, 123516 (2014).
[58]*Elements of Metallurgy and Engineering Alloys*, edited by F. C. Campbel (ASM International, 2008).